Aeroelastic trajectory selection of vortex gusts impinging upon Joukowski airfoils

Huansheng Chen* and Justin W. Jaworski † Lehigh University, Bethlehem, Pennsylvania, 18015

The dynamic interactions between an incident line vortex and a symmetric Joukowski airfoil on elastic translational support are formulated analytically and evaluated numerically, where the unsteady shedding of vorticity from the airfoil trailing edge is modeled by the emended Brown and Michael equation. This mathematical framework explores the effects of initial vortex placement, vortex strength, and the system aeroelastic parameters on the selection of the vortex trajectory to pass either above or below the airfoil, where special attention is paid to the conditions where direct impingement occurs.

I. Introduction

Two-dimensional vortex-structure interactions have received considerable attention over the past decades and have been studied analytically, numerically and experimentally. Doligalski, Smith, and Walker [1] reviewed the model problem of a two-dimensional vortex in a uniform flow above an infinite plane wall, including scenarios where viscous wall interactions become important. An inviscid model of vortex-airfoil interactions is presented by Panaras [2], where he studied the effects of the distance of the vortex from the surface of the airfoil, as well as the effects of vortex size using collections of point vortices. Conlisk and collaborators examined the interactions of a single vortex in a flow with fixed bodies including a corner [3] and a step [4]. Another important two-dimensional vortex-structure interaction problem is a Kármán vortex street encountering a heaving and pitching airfoil, which was examined numerically by Streitlien, Triantafyllou, and Triantafyllou [5]. Vortex-body interaction experiments have provided additional physical insight into the effects of body geometry and placement on vortex impingement and its associated flow physics that are not captured by elementary analytical models. Ziada and Rockwell [6] studied patterns of deformation of incident vortex from the visualization of vortices impinging upon the leading edge of a wedge. Similar leading edge vortex-interactions were studied by Gursul and Rockwell [7], where the interaction of a Kármán vortex street with an elliptical edge was investigated experimentally.

Among the analytical and numerical simulation of vortex-structure interaction, Howe's emended Brown and Michael equation [8] has become a powerful tool to estimate the unsteady shedding of vorticity from aerodynamic bodies. The model supposes that the shed vorticity rolls up via a connecting vortex sheet into a point vortex with varying strength and position that can be described by a set of ordinary differential equations. Interactions between vortex and different aerodynamic bodies, such as surface steps, a duct exit, and an airfoil flap have been studied by Howe [9], Kuo and Dowling [10], and Manela and Huang [11], respectively, using the emended Brown and Michael vortex shedding model. Michaelin and Llewellyn Smith employed the Brown and Michael equation to investigate the aeroelastic vortex-structure dynamics of falling cards [12] and the dynamic instability of flexible membranes in a uniform flow [13]. Recent work by Wang and Eldredge [14] developed a new vortex evolution equation, for which the Brown and Michael framework is a special case.

The present work models the aeroelastic interactions between an incident line vortex and a Joukowski airfoil on an elastic suspension in a uniform flow field. The vortex-airfoil framework of Chen [15] is employed to study the effects of initial vortex position, airfoil vortex shedding, and airfoil motions on the trajectory of the incident vortex. To achieve this goal, the conformal mapping of a Joukowski airfoil and corresponding stream function and complex potential of the flow must be determined. The motion of shed vortex obeys the Brown-Michael equation, and the motions of all the vortices for airfoil on elastic support must be coupled to the airfoil motion, which is governed by a harmonic oscillator equation driven by the unsteady airfoil lift. The present work studies the selection of vortex gusts impinging upon a Joukowski airfoil under aeroelastic motions by inferring the boundary between paths that go either above or below the moving airfoil. The effect of different aeroelastic dimensionless parameters is studied on the selection of the initial incident vortex location to infer when vortex impingement occurs.

^{*}Ph.D. Student, Department of Mechanical and Mechanics, Student Member AIAA

[†]Assistant Professor, Department of Mechanical and Mechanics, Senior Member AIAA

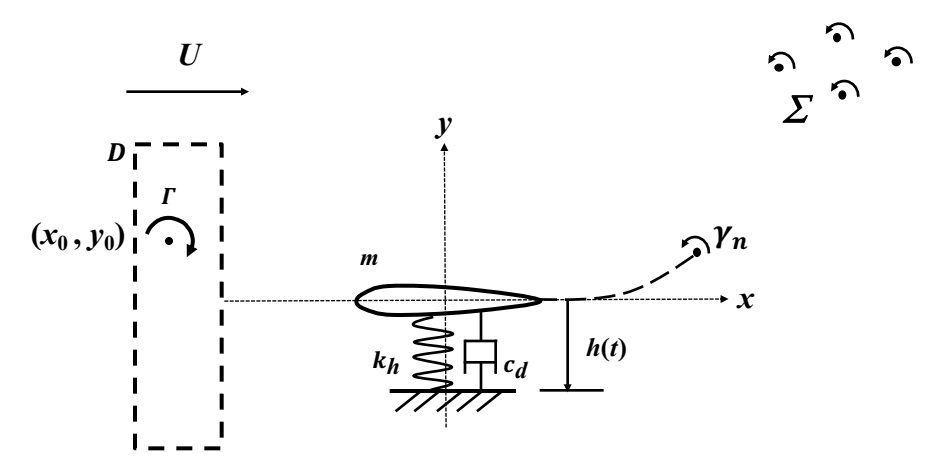


Fig. 1 Schematic of the generalized model problem of an incident vortex interaction with a symmetric Joukowski airfoil on elastic translational support in a uniform flow, where U is the flow speed and h(t) denotes the displacement of the airfoil. The airfoil can be considered as a damped harmonic oscillator with mass m, damping coefficient c_d , and spring stiffness k_h . Γ denotes the incident line vortex located at (x_0, y_0) , and γ_n is the tethered trailing-edge vortex whose motion is determined by the emended Brown and Michael equation. Σ is the set of free vortices generated at the airfoil trailing edge due to unsteady airfoil loads in response to the incident line vortex or airfoil motion. The airfoil has zero angle of attack. D is the initial position selection region of the incident line vortex that travels toward the airfoil.

II. Mathematical formulation

This section outlines the mathematical modeling to describe a Joukowski airfoil in two-dimensional uniform flow with an incident line vortex and shed vorticity field, as illustrated in Fig. 1. The schematic directs the mathematical modeling to of a Joukowski airfoil on elastic supports that encounters a line vortex Γ and sheds a trailing-edge vortex γ_n , whose strength satisfies the Kutta condition and whose motion obeys the emended Brown and Michael equation [8]. Σ denotes the entire vorticity field. The mathematical formulation of the aeroelastic system is now described.

A. Mapping

The conformal mapping of the Joukowski airfoil in the physical z-plane and the mapped ζ -plane is described by

$$\zeta(z) = \frac{1}{2} \left(z + \sqrt{z^2 - 4\lambda^2} \right) - f_0. \tag{1}$$

Using Eq. (1), the Joukowski airfoil in the physical z-plane (z = x + iy) with its trailing edge locating at (2λ , 0) is mapped in a circle f-plane ($f = f_1 + if_2$) with a radius r = 1 (see Fig. 2). Note that the offset of the circle center at $f_0 = f_{x0} + if_{y0}$ and the corresponding trailing edge at (λ , 0). For symmetric Joukowski airfoils, which are considered in this work, $f_{y0} = 0$. The circle in f-plane is then mapped into the same unit circle with its origin at (0,0) in ζ -plane ($\zeta = \xi + i\eta$), and the corresponding trailing edge is at $\lambda - f_0$.

When time-dependent airfoil motions are considered, Eq. (1) becomes

$$\zeta(s) = \frac{1}{2} \left[s(z,t) + \sqrt{s^2 - 4\lambda^2} \right] - f_0, \qquad s(z,t) = z - ih(t).$$
 (2)

B. Flow complex potential

The complex potential of the flow is

$$w(\zeta) = w_{\gamma} + w_{\Gamma} + w_{h} + U\left(\zeta + f_{0} + \frac{\lambda^{2}}{\zeta + f_{0}}\right). \tag{3}$$

where $w_{\gamma}(\zeta)$, $w_{\Gamma}(\zeta)$, and $w_{h}(\zeta)$ are the contributions due to the shed and free vorticity field, the incident vortex, and the airfoil motion, respectively. The last term of Eq. (3) represents the uniform background flow. The complex potentials

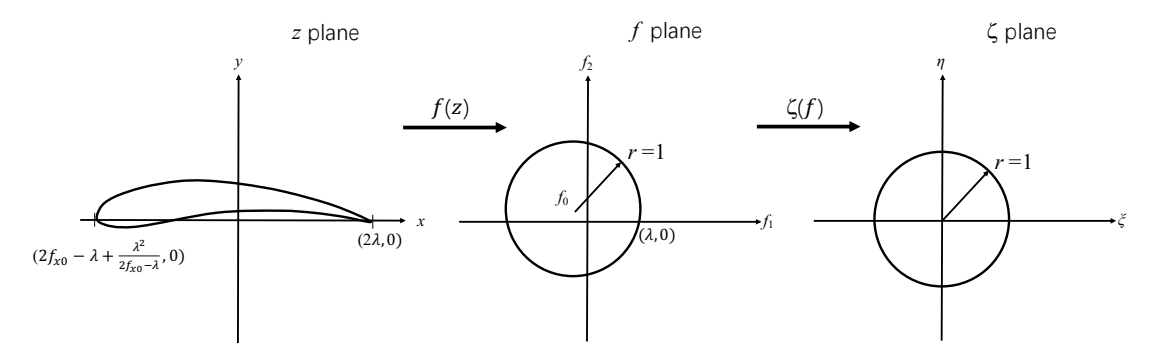


Fig. 2 Successive mappings of a Joukowski airfoil in the physical z-plane to a unit circle centered at the origin in the ζ -plane

are obtained using the mapping introduced in Eq. (1), which yields

$$w_{\Gamma}(\zeta) = -\frac{i\Gamma}{2\pi} \log\left(\zeta - \zeta_{\Gamma}\right) + \frac{i\Gamma}{2\pi} \log\left(\zeta - \frac{1}{\zeta_{\Gamma}^{*}}\right) - \frac{i\Gamma}{2\pi} \log\zeta,\tag{4}$$

$$w_{\gamma}(\zeta) = \sum_{k=1}^{n} \left(-\frac{i\gamma_{k}}{2\pi} \log\left(\zeta - \zeta_{\gamma_{k}}\right) + \frac{i\gamma_{k}}{2\pi} \log\left(\zeta - \frac{1}{\zeta_{\gamma_{k}}^{*}}\right) \right), \tag{5}$$

$$w_h(\zeta) = iV\left(\zeta - \frac{1}{\zeta}\right),\tag{6}$$

where V = dh/dt is the vertical velocity of the motion of the airfoil [16].

C. Vortex shedding and the emended Brown and Michael equation

The motions of the shed vortices are determined by the emended Brown and Michael equation [8],

$$\frac{d\mathbf{x}_{\gamma_n}}{dt} \cdot \nabla \Psi_j + \frac{\Psi_j}{\gamma_n} \frac{d\gamma_n}{dt} = \mathbf{v}_{\gamma_n} \cdot \nabla \Psi_j, \qquad j = 1, 2, \tag{7}$$

where x_{γ_n} represents the location of a shed vortex tethered to the trailing edge with circulation γ_n in a vector form with respect to the rectangular coordinate system $x \equiv (x, y)$. $\Psi_j(x, t)$ denotes the stream function of complex potential of the flow in the j-direction, and v_{γ_n} is the fluid velocity when the local velocity induced by γ_n is excluded. Equation (7) can be rearranged into the equivalent scalar form

$$\frac{dz_{\gamma_n}^*}{dt} + (H_1 - iH_2) \frac{1}{\gamma_n} \frac{d\gamma_n}{dt} = v_{\gamma_n}^*,\tag{8}$$

where $z_{\gamma_n}^* = x - iy$, and $v_{\gamma_n}^* = v_x - iv_y$, H_1 and H_2 are expressions including the stream function Ψ_j and its derivative in j direction, respectively. Here,

$$v_{\gamma_n}^* = -\frac{i\gamma_n \zeta''(z_{\gamma_n})}{4\pi \zeta'(z_{\gamma_n})} + F_{\gamma_n}'(z_{\gamma_n}). \tag{9}$$

Equation (8) is the general scalar form of the emended Brown and Michael equation, which is employed for the theoretical analyses in this work. Specific details related to the derivation of Eq. (8) and the expressions of H_1 and H_2 are tabulated in the Appendix of [17].

For a Joukowski airfoil mapped into the ζ -plane, the components of the stream function are [18]

$$\Psi_1 = \operatorname{Im} \left\{ \zeta + \frac{1}{\zeta} \right\} \quad \text{and} \quad \Psi_2 = \operatorname{Im} \left\{ -i \left(\zeta - \frac{1}{\zeta} \right) \right\}.$$
(10)

The instantaneous circulation of the tethered vortex $\gamma_n(t)$ is obtained by enforcing the Kutta condition at the trailing edge of each instant in time,

$$\gamma_n(t) = \frac{|T^*\zeta_{\gamma_n} - 1|^2}{|\zeta_{\gamma_n}|^2 - 1} \left(\frac{2\Gamma(1 - \text{Re}\{T^*\zeta_{\Gamma}\})}{|T^*\zeta_{\Gamma} - 1|^2} - \sum_{k=1}^{n-1} \gamma_k \frac{|\zeta_{\gamma_k}|^2 - 1}{|T^*\zeta_{\gamma_k} - 1|^2} - 2\pi V \text{Re}(T^*) \right), \tag{11}$$

in which T^* is complex conjugate of the trailing edge T location ($T = \lambda - f_0$) in the ζ -plane. The tethered trailing-edge vortex is released and becomes a free vortex when $d\gamma_n/dt$ changes sign, at which time another tethered vortex is placed at the airfoil trailing edge, whose motion and circulation are determined by Eq. (7) and Eq. (11), respectively.

D. Dynamical formulation

1. Kinematics of the incident and free vortices

The complex velocity of the incident line vortex at s_{Γ} is [19]

$$\frac{ds_{\Gamma}^*}{dt} = -\frac{i\Gamma\zeta''(s_{\Gamma})}{4\pi\zeta'(s_{\Gamma})} + F'(s_{\Gamma}),\tag{12}$$

where

$$F_{\Gamma}'(s_{\Gamma}) = \frac{i\Gamma}{2\pi} \frac{\zeta_{\Gamma}'}{(\zeta_{\Gamma}^2 - 1)\zeta_{\Gamma}} - \frac{i\zeta_{\Gamma}'}{2\pi} \sum_{k=1}^{n} \gamma_k \left(\frac{1}{\zeta_{\Gamma} - \zeta_{\gamma_k}} - \frac{1}{\zeta_{\Gamma} - 1/\zeta_{\gamma_k}^*} \right) + 1. \tag{13}$$

Similarly, the equations of motion for the n-1 free vortices are determined

$$\frac{ds_{\gamma_k}^*}{dt} = -\frac{i\gamma_k \zeta''(s_{\gamma_k})}{4\pi \zeta'(s_{\gamma_k})} + F'_{\gamma_k}(s_{\gamma_k}),\tag{14}$$

where

$$F_{\gamma_{k}}'(s_{\gamma_{k}}) = \frac{i\Gamma}{2\pi} \zeta_{\gamma_{k}}' \left(\frac{1}{\zeta_{\gamma_{k}} - \zeta_{\Gamma}} - \frac{1}{\zeta_{\gamma_{k}} - 1/\zeta_{\Gamma}^{*}} + \frac{1}{\zeta_{\gamma_{k}}} \right) + \frac{i\gamma_{k}}{2\pi} \frac{\zeta_{\gamma_{k}}'}{\zeta_{\gamma_{k}} - 1/\zeta_{\gamma_{k}}^{*}} - \frac{i\zeta_{\gamma_{k}}'}{2\pi} \sum_{m=1, m \neq k}^{n} \gamma_{m} \left(\frac{1}{\zeta_{\Gamma_{k}} - \zeta_{\gamma_{m}}} - \frac{1}{\zeta_{\gamma_{k}} - 1/\zeta_{\gamma_{m}}^{*}} \right) + 1.$$
(15)

2. Airfoil motion and loads

The airfoil moves aeroelastically under the lift force and the equation of motion of the elastic mount. The lift force on a thin airfoil can be decided by [20]:

$$L' = \int_0^c \rho \left[U\gamma(x,t) + \frac{\partial}{\partial t} \Gamma_a(x,t) \right] dx$$
$$= \rho U\Gamma_a(t) + \rho \int_0^c \frac{\partial}{\partial t} \Gamma_a(x,t) dx \tag{16}$$

where the first term is the quasi-steady lift due to the instantaneous circulation, and the second term denotes the time-dependent contribution of the lift due to the airfoil motion and the downwash effect of the wake.

The quasi-steady circulation Γ_a in the first term can be decided in agreement with Kelvin's theorem

$$\Gamma_a(t) = \sum_{k=1}^{n} \gamma_k(t) \tag{17}$$

which satisfies no airfoil circulation when t = 0, and γ_k denotes the strength of the k^{th} shed vortex.

The general formulation of the airfoil circulation $\Gamma_a(x,t)$ is determined by [20]:

$$\Gamma_a(x,t) = \int_0^c \gamma(x,t)dx \tag{18}$$

where $\gamma(x, t)$ is the vorticity distribution on the airfoil.

The vorticity distribution may be analytically rewritten as a trigonometric expansion of the following from [21]:

$$\gamma(x,t) = 2U \left[A_0(t) \frac{1 + \cos \theta}{\sin \theta} + \sum_{n=1}^{\infty} A_n \sin n\theta \right], \tag{19}$$

where the first term in the bracket is the vorticity distribution for the symmetric airfoil, and the second term summation reflects to the camber distribution. For a symmetric airfoil, only $A_0(t)$ is not identically zero at all times.

In terms of the coefficients A_0 and A_n , Eq. (16) can be expanded as

$$L' = \pi \rho c \left\{ \left[U^2 A_0 + \frac{3c}{4} \frac{\partial}{\partial t} (U A_0) \right] + \left[U^2 \frac{A_1}{2} + \frac{c}{4} \frac{\partial}{\partial t} (U A_1) + \frac{c}{8} \frac{\partial}{\partial t} (U A_2) \right] \right\}$$
$$= \rho U \left[\pi c U \left(A_0 + \frac{A_1}{2} \right) \right] + \pi \rho c^2 U \left(\frac{3}{4} \frac{\partial A_0}{\partial t} + \frac{1}{4} \frac{\partial A_1}{\partial t} + \frac{1}{8} \frac{\partial A_2}{\partial t} \right)$$
(20)

where the first term is equivalent to the quasi-steady lift in Eq. (16), and the second term is equivalent to the lift contribution due to time dependency. Details of this expansion can be found in [20].

The elastic suspension is represented by a spring-damper system, and the airfoil motion is governed by the ordinary differential equation

$$m\frac{d^2h}{dt^2} + c_d\frac{dh}{dt} + k_h h = -L', (21)$$

where h(t) denotes the displacement of the airfoil, and the airfoil can be considered as a damped harmonic oscillator with mass m, damping coefficient c_d , and spring stiffness k_h , and L' is the lift of the airfoil.

Equation (21) can be rewritten as

$$\frac{d^2h}{dt^2} + 2\omega_n \xi \frac{dh}{dt} + \omega_n^2 h = -\frac{L'}{m},\tag{22}$$

with

$$c_d = 2m\omega_n \xi,\tag{23}$$

and

$$k_h = m\omega_n^2, (24)$$

where $\omega_n = \sqrt{k_h/m}$ is the natural frequency of the harmonic oscillator, ξ is the damping ratio of the system.

Equation (22) may be put into dimensionless form using the following scalings: $\overline{x} = x/2\lambda$, $\overline{y} = y/2\lambda$, $\overline{t} = Ut/2\lambda$, $\overline{\Gamma} = \Gamma/(4\pi U\lambda)$, and $\overline{\omega}_n = 2\omega_n\lambda/U$. With these scalings, a mass ratio μ can be defined,

$$\mu = \frac{m}{m_f},\tag{25}$$

where m is the approximate mass of the airfoil:

$$m = \rho_a l_t c, \tag{26}$$

and m_f is apparent mass of the fluid:

$$m_f = \pi \rho \left(\frac{c}{2}\right)^2. \tag{27}$$

Here ρ_a is the average volumetric density of the airfoil, ρ is the fluid density, and c is the chord length of the airfoil in the physical z-plane, and l_t is the thickness of the airfoil.

The parameter space of the elastic suspension is therefore set by three dimensionless quantities: the damping ratio ξ , the reduced natural frequency $\overline{\omega}_n$, and the mass ratio μ . Now Eq. (22) can be nondimensionalized as

$$\frac{d^2\overline{h}}{d\overline{t}^2} + 2\overline{\omega}_n \xi \frac{d\overline{h}}{d\overline{t}} + \overline{\omega}_n^2 \overline{h} = -c_L \frac{2}{\pi \mu \overline{c}},\tag{28}$$

where c_L is the sectional lift coefficient, and \overline{c} is the chord length scaled by 2λ .

The system of dynamical equations is formed from Eqs.(8), (11), (12), (14), and (28), which consists of 2(n+2) first-order ordinary differential equations for the position $(s_{x_{\Gamma}(t)}, s_{y_{\Gamma}(t)})$ of the incident line vortex, the positions $(s_{x_{\gamma_n}(t)}, s_{y_{\gamma_n}(t)})$ of n trailing edge vortices, and the instantaneous airfoil displacement h(t) and velocity V(t). The system of equations is marched forward in time using ODE45 in MATLAB. Once solved, the results are mapped into the physical z-plane by using z(t) = s(t) + ih(t).

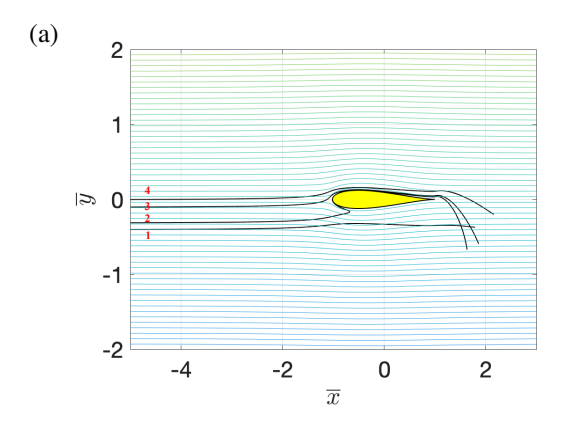
III. Results

The numerical simulations are carried out and are parameterized by the reduced natural frequency, $\overline{\omega}_n = (2\omega_n\lambda)/U$, and incident vortex strength, $\overline{\Gamma} = \Gamma/(4\pi U\lambda)$. The conditions are scaled by 2λ : $\overline{x} = x/(2\lambda)$, and $\overline{y} = y/(2\lambda)$. The simulations are initialized by the the initial shed vortex location, $\overline{z}_{\gamma}(0) = z_{\gamma}(0)/(2\lambda) = (1, 0.000001)$, and the initial x-coordinate of the incident vortex is $\Delta \overline{x} = x_0(0)/(2\lambda) = -20$. The mass ratio is fixed to $\mu = 10$, the airfoil has 12% thickness, and angle of attack is not considered. The structural damping ratio is neglected ($\xi = 0$).

In terms of the initial conditions, the mathematical model is controlled by two dimensionless parameters including the strength of the incident vortex, $\overline{\Gamma}$, and the reduced natural frequency of the oscillator, $\overline{\omega}_n$. Different initial locations of the incident vortex result in the passage of the incident vortex either above or below the airfoil. Here, the bisection method is used to find the initial vortex position $\Delta \overline{y}$ for direct airfoil impingement given $\overline{\Gamma}$ and $\overline{\omega}_n$. For example, with $\Gamma = 0.1$ and $\overline{\omega}_n = 0.5$, set the initial range of \overline{y} to be [-2,2], test if the incident vortex will pass above the airfoil when setting the mid-value of the range to be $\Delta \overline{y}$, then the new range of the \overline{y} is [-2,mid] if the incident vortex passes above the airfoil, [mid,2] if it passes below the airfoil. Finally, the range will home in on the exact $\Delta \overline{y}$ when the vortex impingement happens. The accuracy of $\Delta \overline{y}$ is controlled by the tolerance of the bisection method, which is set to be $\overline{\varnothing} = \varnothing/(2\lambda) = 0.01$ in the present work. The corresponding results can be found in Fig. 3, which shows the incident vortex trajectories for different initial vortex positions and the corresponding time histories of the airfoil circulation, where Fig. 3(a) compares the trajectories of the incident vortex in the aeroelastic simulations with different initial locations including the impingement-occurring location $(\Delta \overline{x}, \Delta \overline{y}) = (-20, -0.31)$ determined by the bisection method, respectively, against the steady streamlines of the flow field in the absence of vortices. For the initial location (20,-0.4), the incident vortex follows initially the steady streamline from the left inflow locations, and moves below the airfoil at large times. As the initial location moves up to the impingement-occurring location (20,-0.31), the incident vortex aligns with the steady streamline at early times. However, near the airfoil, the vortex path deviates backward under influence of the shed vorticity and airfoil motion and moves along a path near the stagnation streamline at the airfoil. As the initial location of the incident vortex moves upward, smaller deviation of the path of the incident vortex is observed in Fig. 3(a).

Figure 3(b) presents the time variations of the airfoil circulation for the shedding of the first two trailing-edge vortices. For the cases when the initial vortex location is (-20,0) and (-20,-0.1), which causes the incident vortex move above the airfoil, the corresponding airfoil circulation time histories increase similarly at early times, and have a sharp change when the incident vortex passes closest to the airfoil due to the shedding of the second vortex and a strong vortex-airfoil interaction. However, for the case when the initial vortex will moves below the airfoil, a small limit and an extended flat response in the airfoil circulation with respect to time can be seen in the dashed line of Fig. 3(b), which may infer a weak interaction between the incident vortex and the airfoil. When the initial vortex location is set to (-20,-0.31), which results in vortex impingement, a similar variation of the airfoil circulation can be observed in the dash-dot line of Fig. 3(b), compared with the solid line and the dotted line. However, the shedding of the second vortex is delayed when the incident vortex passes near the stagnation streamline at the airfoil.

Furthermore, the effects of different aeroelastic parameters such as $\overline{\Gamma}$ and $\overline{\omega}_n$ on the selection of initial incident vortex locations to achieve vortex impingement are studied, respectively. In testing the current numerical scheme, the vortex impingement commonly occurs in the shedding of the first trailing-edge vortex, in which time the downwash effect of the wake may be neglected. In checking of the sensitivity of the numerical scheme to the choice of aerodynamic model, where the more sophisticated full unsteady version becomes more unstable as the vortex approaches the dividing



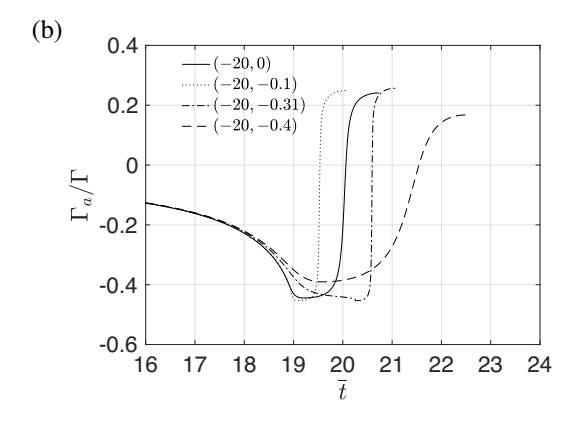


Fig. 3 Time histories of incident vortex trajectories and the bound circulation for different initial vortex positions, with reduced natural frequency $\overline{\omega}_n=0.5$, and the strength of the incident vortex $\overline{\Gamma}=0.1$: (a) time-varying trajectories of the incident line vortex Γ (denoted 1, 2, 3, 4) resulting from an incident vortex Γ with different initial positions at (-20,-0.4), (-20,-0.31), (-20,-0.1), and (-20,0) past along a symmetrical Joukowski airfoil with 12% thickness. The streamlines in the flow field are for the case where all vortices are absent, and the motion of the indicent vortex across these lines under the influence of the airfoil is noted; (b) time variations of corresponding bound circulation on the airfoil during the shedding of the first two trailing-edge vortices.

line between upper and lower trajectories. Therefore, the downwash effect of the wake is neglected in the analysis below and the tolerance of the bisection method is set to be $\overline{\varnothing} = \varnothing/(2\lambda) = 0.01$ in the present work. This tolerance produces accurate results, but the solver developed by the authors did not permit smaller tolerance values due to the sensitivity of the numerical scheme to the complexity of aerodynamic model.

Figure 4 presents results for the vortex initial vertical position to achieve direct airfoil impingement as a function for $\overline{\omega}_n$ for $\overline{\Gamma}=0.1$. In these simulations, the downwash effect of the airfoil wake has been neglected in the aerodynamic model to achieve a reasonable numerical tolerance. It is clear from Fig. 4 that there are upper and lower asymptotic limits on the values of $\Delta \overline{y}$, where $\Delta \overline{y} \to -0.17$ for small values of $\overline{\omega}_n$, and $\Delta \overline{y} \to -0.328$ for large values. Recalling that these simulations are at fixed mass ratio, $\mu=10$, and have no structural damping, $\xi=0$, the lower and upper limits correspond to negligible spring restoring force (free airfoil) and dominant spring (rigid support) limits. Importantly, the results demonstrate a monotonic change in initial vortex position $\Delta \overline{y}$ with respect to the reduced natural frequency for a given value, and these values of $\Delta \overline{y}$ are bounded by the low and high frequency limits in $\Delta \overline{y}$.

Next consider the case of a fixed reduced natural frequency, $\overline{\omega}_n = 0.5$, where the initial incident vortex locations $\Delta \overline{y}$ can be determined as a function of the incident vortex strength $\overline{\Gamma}$, as shown in Fig. 5. In Fig. 5, the monotonically decreasing value of $\Delta \overline{y}$ with increasing $\overline{\Gamma}$ indicates the need for lower vortex positioning for direct impingement for stronger incident vortices.

IV. Conclusions

This paper simulates the aeroelastic interactions of an incident vortex with a symmetric Joukowski airfoil on an elastic suspension. The mathematical framework is extended from previous effort in other work by Chen [17] involving similar vortex shedding models with prescribed airfoil motion. The conditions for achieving direct impingement of an incident line vortex with the elastically-mounted airfoil are determined numerically in this work.

The aeroelastic results of a symmetric Joukowski airfoil with 12% thickness demonstrate that the incident vortex follows initially the steady streamline in the uniform flow, but deviates backward and then moves along a path near the stagnation streamline at the airfoil near where the vortex impingement occurs. The numerical results also indicate weak sensitivity of the vortex initial vertical position to the reduced natural frequency when this frequency is either small or large, but the initial vortex placement for airfoil impingement changes monotonically with the natural frequency in a specific range that depends on the vortex strength.

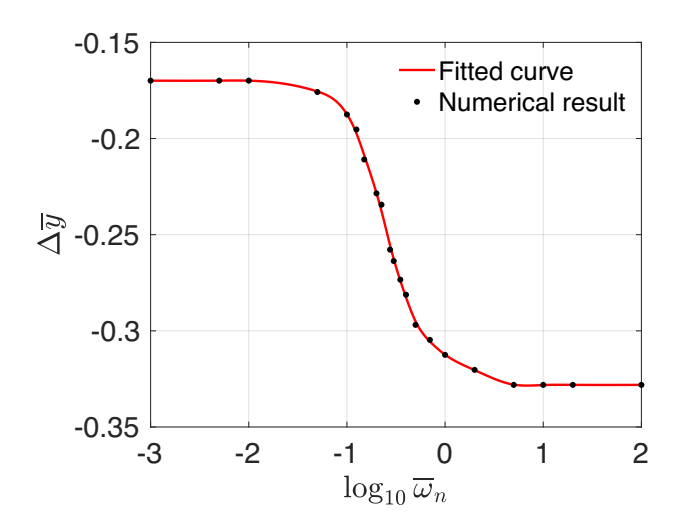


Fig. 4 Effect of reduced natural frequency $\overline{\omega}_n$ on the initial incident vortex vertical position $\Delta \overline{y}$ to achieve direct airfoil impingement. Incident vortex has a strength of $\overline{\Gamma}=$ 0.1 and moves past a symmetric Joukowski airfoil with 12% thickness.

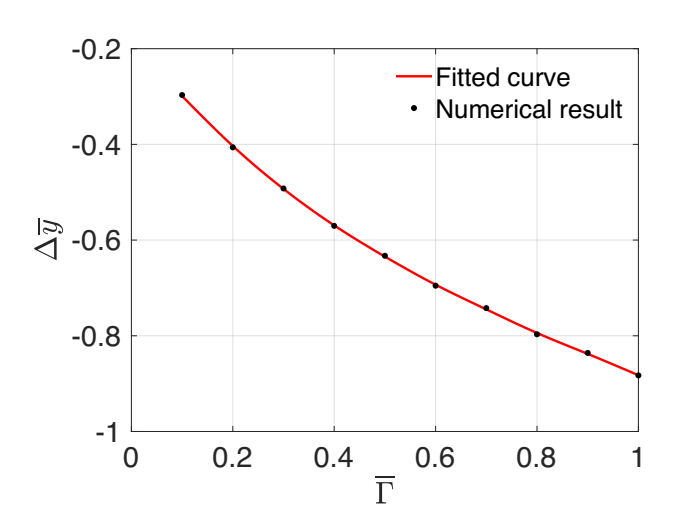


Fig. 5 Variations of selection of initial incident vortex location $\Delta \overline{y}$ with varying strength of incident vortex $\overline{\Gamma}$ when vortex impingement occurs, with reduced natural frequency $\overline{\omega}_n = 0.5$.

8

Acknowledgments

This work was supported in part by the Air Force Office of Scientific Research under AFOSR grant FA9550-15-1-0148, monitored by Drs. Douglas Smith and Gregg Abate, and by the National Science Foundation under award 1805692, monitored by Dr. Ronald Roslin.

References

- [1] Doligalski, T. L., Smith, C. R., and Walker, J. D. A., "Vortex interactions with walls," *Annual Review of Fluid Mechanics*, Vol. 26, No. 1, 1994, pp. 573–616.
- [2] Panaras, A. G., "Numerical modeling of the vortex/airfoil interaction," AIAA Journal, Vol. 25, No. 1, 1987, pp. 5–11.
- [3] Conlisk, A., and Rockwell, D., "Modeling of vortex-corner interaction using point vortices," *The Physics of Fluids*, Vol. 24, No. 12, 1981, pp. 2133–2142.
- [4] Conlisk, A., and Veley, D., "The generation of noise in impinging vortex motion past a step," *The Physics of Fluids*, Vol. 28, No. 10, 1985, pp. 3004–3012.
- [5] Streitlien, K., Triantafyllou, G. S., and Triantafyllou, M. S., "Efficient foil propulsion through vortex control," *AIAA Journal*, Vol. 34, No. 11, 1996, pp. 2315–2319.
- [6] Ziada, S., and Rockwell, D., "Vortex-leading-edge interaction," Journal of Fluid Mechanics, Vol. 118, 1982, pp. 79-107.
- [7] Gursul, I., and Rockwell, D., "Vortex street impinging upon an elliptical leading edge," *Journal of Fluid Mechanics*, Vol. 211, 1990, pp. 211–242.
- [8] Howe, M. S., "Emendation of the Brown & Michael equation, with application to sound generation by vortex motion near a half-plane," *Journal of Fluid Mechanics*, Vol. 329, 1996, pp. 89–101.
- [9] Howe, M. S., "Influence of separation on sound generated by vortex-step interaction," *Journal of Fluids and Structures*, Vol. 11, No. 8, 1997, pp. 857–872.
- [10] Kuo, C.-Y., and Dowling, A. P., "Acoustics of a two-dimensional compact jet impinging normally onto a flat plate," *Journal of Fluid Mechanics*, Vol. 414, 2000, pp. 251–284.
- [11] Manela, A., and Huang, L., "Point vortex model for prediction of sound generated by a wing with flap interacting with a passing vortex," *The Journal of the Acoustical Society of America*, Vol. 133, No. 4, 2013, pp. 1934–1944.
- [12] Michelin, S., and Llewellyn Smith, S. G., "An unsteady point vortex method for coupled fluid–solid problems," *Theoretical and Computational Fluid Dynamics*, Vol. 23, No. 2, 2009, pp. 127–153.
- [13] Michelin, S., and Llewellyn Smith, S. G., "Falling cards and flapping flags: understanding fluid–solid interactions using an unsteady point vortex model," *Theoretical and Computational Fluid Dynamics*, Vol. 24, No. 1-4, 2010, pp. 195–200.
- [14] Wang, C., and Eldredge, J. D., "Low-order phenomenological modeling of leading-edge vortex formation," *Theoretical and Computational Fluid Dynamics*, Vol. 27, No. 5, 2013, pp. 577–598.
- [15] Chen, H., "Vortex gust interactions with oscillating Joukowski airfoil," Master's thesis, Lehigh University, May 2018.
- [16] Batchelor, G. K., An Introduction to Fluid Dynamics, Cambridge University Press, United Kingdom, 1967.
- [17] Chen, H., and Jaworski, J. W., "Vortex interactions with Joukowski airfoil on elastic supports," AIAA Fluid Dynamics Conference, Atlanta, GA, Paper AIAA-2018-2907, 2018.
- [18] Howe, M. S., Acoustics and Aerodynamic Sound, Cambridge University Press, United Kingdom, 2014.
- [19] Howe, M. S., Hydrodynamics and Sound, Cambridge University Press, United Kingdom, 2006.
- [20] Katz, J., and Plotkin, A., Low-speed aerodynamics, Vol. 13, Cambridge University Press, United Kingdom, 2001.
- [21] Glauert, H., The elements of aerofoil and airscrew theory, Cambridge University Press, United Kingdom, 1983.

Correction: [Aeroelastic trajectory selection of vortex gusts impinging upon Joukowski airfoils]

Author(s) Name: Huansheng Chen, Justin W. Jaworski

Author(s) Affiliations: Lehigh University, Bethlehem, Pennsylvania, 18015

Correction Notice

The following missing term should be added on the right side of equation (13):

$$iV\zeta'_{\Gamma}(1+\frac{1}{\zeta_{\Gamma}^2})$$

The following missing term should be added on the right side of equation (15): $iV\zeta'_{\gamma_k}(1+\frac{1}{\zeta^2_{\gamma_k}})$

$$iV\zeta'_{\gamma_k}(1+\frac{1}{\zeta^2_{\gamma_k}})$$

In equation (19), $x = \frac{c}{2}(1 - \cos\theta)$ and $\gamma(x, t)$ should be written as $\gamma(\theta, t)$